CONSTRAINING PRESENT-DAY INTERNAL STRUCTURE OF THE MOON WITH IMPLICATIONS FOR ITS FORMATION USING THERMOELASTIC EQUATIONS OF STATE MODELING. A. Mallik[1], H. Fuqua Haviland[2**], P. M. Bremner[3], M. Diamond[4], and the 2014 CIDER Moon Group[5]. [1]University of Rhode Island, [2]NASA Marshall Space Flight Center (heidi.haviland@nasa.gov), [3]Univerisity of Florida, [4]University of California, Berkeley, [5]Cooperative Institute for Dynamic Earth Research (www.deep-earth.org). [**]Presenting author.

Introduction: The existence of a partially molten layer deep within the Moon's mantle has been proposed to explain the lack of observed far-side deep moonquakes [1], the observation of reflected phases from deep moonquakes [2], and the dissipation of tidal energy within the lunar interior [3]. However, subsequent models have proposed that dissipation due to elevated temperatures alone can explain the observed dissipation factor and tidal Love numbers [4]. In this study we used thermoelastic modeling to explore the hypothesis that an ilmenite-rich layer formed just below the crustal anorthosite during magma ocean crystallization and may have sunk to the base of the mantle to create a partial melt layer at the core-mantle boundary. We performed nearly 400,000 forward calculations by varying the thicknesses of proposed chemically and mineralogically distinct layers within the Moon and compared the resultant masses and moments of inertia (MOI) with those determined by GRAIL in order to constrain large-scale lunar structure, as well as to evaluate if an ilmenite-rich partially molten layer at the base of the lunar mantle is well constrained by the Apollo seismic data. This multidisciplinary analysis approach has yielded key insights into the lunar interior structure, thermal state, and formation history.

Methods: Self-consistent physical parameters are calculated for three mantle compositional models: a mantle with preserved mineralogical stratigraphy from lunar magma ocean (LMO) crystallization, and two well-mixed compositionally homogeneous mantles with uniform bulk composition from [5, 6], Fig. 1. For both of these homogeneous cases, each layer's equilibrium phase assemblage was computed using the thermodynamic modeling software pMELTS. The crust is fixed at 40 km thick–the average crustal thickness from GRAIL [7]. All other layer thicknesses are varied. We include the possibility of an Fe-Ti-rich layer at both the top and bottom of the mantle to test the origin and existence of a residual ilmenite-rich layer below the anorthite crust after gravitational overturn and a partial melt layer at the core mantle boundary as a consequence of overturn, respectively. Our core consists of a liquid-iron outer core and a solid-iron inner core.

Additionally, we considered cold, medium, and hot lunar temperature profiles, or selenotherms, which bound the published profiles derived from seismic, electromagnetic, and gravity data [8, 9, 10]. These parameters were compared against observed mass, MOI, bulk chemistry, and published seismic velocity profiles. We forward calculated lunar compositional models by varying the thicknesses of stratigraphic layers within the starting model and calculating self-consistent physical parameters through equation of state modeling via the mineral physics software toolkit Burnman [11]. Generation of specific stratigraphic layer thicknesses proceeded in three steps to robustly explore parameter space: a grid search, random model generation, and lastly a differential evolution search [12] guided by minimizing the misfit from GRAIL mass and MOI [13]. From the three compositional starting models each with three selenotherms, we considered nine composition-temperature classifications, each with ~45,000 generated models. Furthermore, we compared the resulting bulk chemistry of each generated model, in SiO_2-TiO_2-Al_2O_3-FeO-MgO-CaO space, to the average of twenty-six bulk chemistry models currently published for the Moon. Lastly, we compared our models to the Weber and Garcia seismic profiles [2, 14] for understanding into how our models are constrained by Apollo seismic observations. We made the following assumptions: the compositional layers are radially averaged to be globally homogeneous, thus the near and far side hemispherical dichotomies (i.e., crustal thickness, composition) are beyond the scope of this current study; and, secondly, we do not consider the regolith which likely affected surface heat flow measurements, as well as seismic wave propagation.

Conclusions: We obtained the following key results from the analysis of our models: (1) Both homogeneous and stratified compositional models are able to satisfy mass and MOI leading to the necessity of additional constraints to distinguish this model space. Homogenous models require a warm-to-hot selenotherm. (2) The Moon must have a small (200-400 km) dense metallic core. (3) Models that fit mass and MOI have thin or no "upper" ilmenite-rich layer preserved just below the crust and a "lower" ilmenite-rich layer is present, consistent with an overturn scenario. Whether the "lower" ilmenite-rich layer is partially molten depends on CMB temperature. (4) We found that it is possible to reasonably fit the published seismic profiles with all three selenotherms (cold, medium, and hot), and that mass and MOI are more sensitive than seismic velocity to temperature.

Fig. 1. (*below*) Geochemically informed starting compositional models are defined by distinct mineralogical layers considering three end member scenarios: (*right*) Compositionally Stratified mineralogy preserves LMO crystallization stratigraphy, with the upper 400 km containing mantle cumulate compositions as a function of percentage of magma ocean (MO) crystallization [15], and the lower mantle (400 - 1400 km depth) based on the cumulate pile after 50% MO crystallization of a bulk mantle from [6], as reported by [16]. (*left and center*) We consider two cases with homogenous mantle bulk compositions in which the stratified MO layers are erased by sufficient mantle mixing. We start with simplified bulk compositions from [6, *left*] and [5, *center*] for all mantle depths. The mineralogy of the upper and lower ilmenite layers from [15] are: Clinopyroxene (60% He + 14% Di) + Ilmenite (23%) + Anorthite (2%).

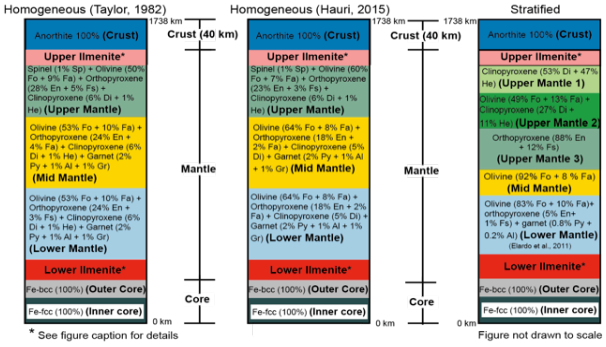

Fig. 2. (*below*). The total model count distribution as a function of fit to mass and MOI. The x-axis and y-axis are the standard deviation misfits from observed mass and MOI, respectively. The colors indicate the distribution of the number of models that achieved a mass or MOI misfit. The range of mass and MOI misfits covered demonstrate a very large geophysical model space was explored with a wide range of input parameters. The pink star represents the Garcia model [14], and green star is the Weber model [2].

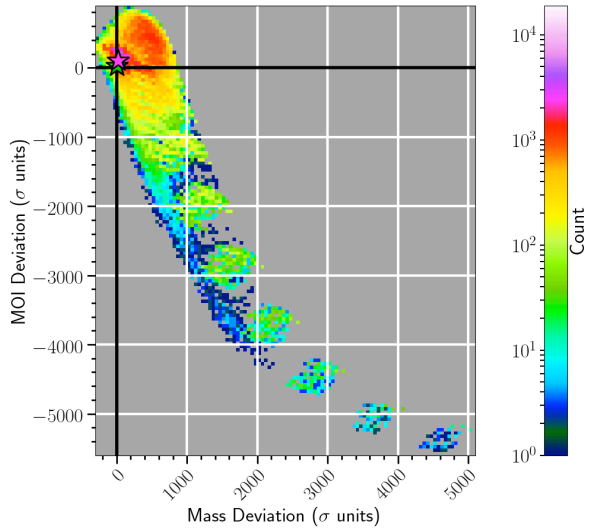

Fig. 3. (*below*). The total (inner+outer) core thickness as a function of L2-norm, or the square root of the normalized mass and MOI misfits, for each of the nine model classifications. Each generated lunar model is represented by a horizontal line whose length and color both scale with the L2-norm value. Darker, longer lines equala larger L2-norm (worse fit); lighter, shorter lines equal a smaller L2-norm, (better fit). Shorter lines are on top of longer lines. The left-hand side of each column of horizontal lines depicts the range of core thicknesses within 3 sigma (black box), 1 sigma (white box), and the full extent of thicknesses considered (whiskers). The red bar indicates the best fit model for each classification. Across all nine model classifications our models require a core of 200-400 km to meet the mass and MOI, and trend toward decreasing core size with decreasing temperature. This is consistent with other studies of the lunar core from electromagnetic and seismic data. We also see that cooler models have a distinctly narrower range of core size. CH – Compositionally homogeneous models. CS – Compositionally stratified models.

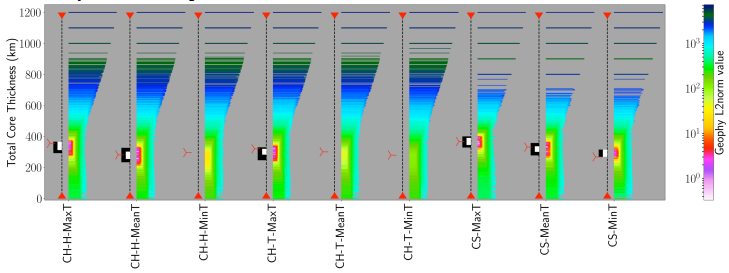

References: [1] Nakamura, Y. (2005). *JGR.* 110, 1–12. [2] Weber, R. C., et al. (2011). *Science (80-.).* 331, 309–312. [3] Williams, J. G., et al. (2001). *JGR.* 106, 27933. [4] Nimmo, F., et al. (2012). *JGR.* 117, E09005. [5] Hauri, E. H., et al. (2015). *EPSL.* 409, 252–264. [6] Taylor, S. R. (1982). *Phys. Earth Planet. Inter.* 29, 233–241. [7] M.A. Wieczorek, et al., *Science*. 339 (2013) 671–5. [8] Gagnepain-Beyneix, J., et al. (2006). *Phys. Earth Planet. Inter.* 159, 140–166. [9] Khan, A., et al. (2006). *EPSL.* 248, 579–598. [10] Khan, A., et al. (2007). *GJI.* 168, 243–258. [11] Cottaar, S., et al. (2014). *GGG* 15.4, 1164–1179. [12] K. V. Price, R.M. Storn, (2005) 538. [13] Williams, J. G. et al. (2014). *JGR-P.* 119, 1546–1578. [14] Garcia, R. F. et al. (2011). *Phys. Earth Planet. Inter.* 188, 96–113. [15] Snyder, G. A., et al. (1992). *GCA.* 56, 3809–3823. [16] Elardo, S. M., et al. (2011) *GCA.* 75, 3024–3045.

Additional Information: We gratefully acknowledge the grant *CIDER-II, Frontiers of Earth Systems Dynamics (FESD), NSF, grant#EAR-1135452,* for its support of this work.